THE DIATOMICS-IN-MOLECULES METHOD AS A MEANS FOR PREDICTING POTENTIAL-ENERGY-SURFACE TOPOLOLOGY. A CASE STUDY FOR THE REACTION OF C^+ WITH O_2

Rudolf POLAK

J. Heyrovsky Institute of Physical Chemistry, Academy of Sciences of the Czech Republik, 182 23 Prague 8, Czech Republic; e-mail: polak@jh-inst.cas.cz

Received May 18, 1998
Accepted May 25, 1998

Dedicated to Professor Rudolf Zahradnik on the occasion of his 70th birthday.

Energy correlation diagrams constructed by means of a Diatomics-in-molecules model, based on the minimum basis of atomic states, indicate some unexpected features of the potential energy surfaces governing the $C^+ + O_2$ reaction. Confirmation of the early down-hill character of doublet surfaces and the presence of potential wells in C_{2v} configurations could rise new aspects of the dynamics and mechanism of the reaction, because it is believed that entrance channel effects are very important in this reaction.

Key words: Diatomics-in-molecules method; Valence bond structures; Doublet and quartet states of $(CO_2)^+$; Energy correlation diagrams; Topology of potential energy surfaces; *Ab initio* calculations.

The originally outlined area of applicability of Ellison's Diatomics-in-molecules (DIM) method[1] consisted of three items: To predict stabilities of polyatomic molecules, to provide understanding of deviations from strict additivity of bond energies, and to give semiempirical explanation for nonbonded interactions. Soon after the invention of the method it has been recognized[2,3] that DIM is most usefully practicable in molecular collision theory work, as a tool for providing physically justified approximations for potential energy surfaces (PESs) in dynamics calculations. All shortcomings and advantages of this method emerge from specific approximations inherent in the DIM approach which allow to look upon the properties of the polyatomic system as the resultant of ground and excited diatomic state interactions. Despite the fact that DIM has no power of being quantitatively correct and not-mistakenly predictive at any situation, there are two important directions of its application.

The first one consists in using DIM as a *fitting scheme*, having the ability to match the overall features of the accurate PES, without losing the correct behaviour in the reactant and product regions of the reaction system. In simplest instances, for which $(HeH_2)^+$ is the prototype[4], the DIM formulation leads to a London–Eyring–Polanyi–Sato-type

procedure[5–7] where excited state diatomic interaction curves can be adjusted to achieve a consistent representation of the ground state PES. In more complex DIM models, additional possibilities exist to optimize the DIM solution *via* alteration of interactions within state manifolds of diatomic species of equal spin- and space-symmetry. Mainly because of computational reasons, DIM as a fit function has been for a long time confined only to modest models (*e.g.* refs[8–12]), being characteristic of small dimensions of both the polyatomic and diatomic fragment basis sets. Recently, however, it has been shown that even complex DIM models are amenable to manipulation for obtaining physically realistic representations of PESs, simultaneously for ground and excited electronic states[13,14].

Applications of DIM, that might be placed in the second category, are related to the *qualitative characterization of chemical reactions and prediction of PES topology*, with main emphasis to barriers, wells, surface real and avoided crossings *etc*., conveniently manifested by appropriate correlation diagrams. An apt example to this sort of problem is providing the DIM study of the O + H_2 reaction[11], detecting PES intersections on the reaction pathway which were not known before from *ab initio* calculations.

In this paper we want to investigate the reactions $C^+(^2P_u)$ + $O_2(X\ ^3\Sigma_g^-) \rightarrow O^+(CO)$ and $CO^+(O)$ which play a major role in gas-phase-, plasma- and combustion-processes, and have been studied experimentally by various techniques (see refs[15–18] and references therein). In order to discuss the experimental results in terms of reaction mechanisms and to rationalize the wealth of data on this reaction system, there have been applied electronic state correlation diagrams[15–18] based on the contemporary knowledge of the pertinent PESs. Since only limited theoretical data were available, and because of the complicated pattern of many surfaces and their intersections, a great deal of surface features entering the diagrams were tentative or created on grounds of molecular orbital correlations. Therefore, we decided to reinvestigate the overall topographical behaviour of the low-lying doublet and quartet states of $(CO_2)^+$ by means of a DIM model with a hope to receive a picture of adiabatic correlations between reactant, intermediate and product states which would be useful in giving clues to sophisticated *ab initio* approaches for the search of critical features of the PESs not yet discovered.

THEORETICAL

DIM Models for Doublet and Quartet States of $(CO_2)^+$

The DIM model structure[19] for the doublet and quartet states of the $(CO_2)^+$ system is specified by the selection of atomic states, O ^3P_g (p^4), O^+ ^4S_u (p^3) and C ^3P_g (p^2), C^+ ^2P_u (p), which combine to form three state groups (SGs) indicated in Table I. Each state group yields a direct-product sub-set of three-atomic basis functions (TBFs) which, in case of the absence of spin–orbit interaction, can be written in the form of a product of spatial and spin parts. For a given SG, the spatial part of an individual basis function is char-

acterized by a set $[m(1),m(2),m(3)]_{SG}$ of quantum numbers $m(i)$ referring to the electronic (spatial) angular momentum projection of atom i (i = 1, 2, 3), and the spin parts correspond to all linearly independent spin-adapted polyatomic basis functions with total spin quantum numbers S and M_S which can be constructed from a given combination of atomic terms. For example, there are two independent total doublet (S = 1/2, M_S = 1/2) functions σ_i corresponding to SG (a), namely

$$\begin{bmatrix} {}^{(a)}\sigma_1 \\ {}^{(a)}\sigma_2 \end{bmatrix} = \begin{bmatrix} 0 & 1/\sqrt{3} & 0 & -1/\sqrt{3} & 1/\sqrt{3} \\ -1/\sqrt{3} & 1/\sqrt{6} & 1/\sqrt{3} & 0 & -1/\sqrt{6} \end{bmatrix} \begin{bmatrix} \{1, 0, -1/2\} \\ \{-1, -1, 1/2\} \\ \{0, 1, -1/2\} \\ \{0, 0, 1/2\} \\ \{-1, 1, 1/2\} \end{bmatrix} \quad (1)$$

where $\{m_s(1), m_s(2), m_s(3)\}$ denotes a three-atom-product spin function characterized by projection spin quantum numbers of individual atomic states. Notice that ${}^{(a)}\sigma_1$ and ${}^{(a)}\sigma_2$ are symmetric and antisymmetric with regard to the permutation of atoms 1 and 2, respectively. Further, ${}^{(a)}\sigma_1$ and ${}^{(a)}\sigma_2$ are eigenfunctions of the 1,2-fragment spin operator $\boldsymbol{S}_{12}^2$ with eigenvalues 0 and 1, corresponding to diatomic singlet and triplet states, respectively. In turn, ${}^{(a)}\sigma_1$ and ${}^{(a)}\sigma_2$ can be transformed by a unitary transformation to

TABLE I
DIM basis functions for doublet and quartet states of $(CO_2)^+$ characterized by quantum numbers S related to eigenvalues of diatomic fragment spin-operators $\boldsymbol{S}_{ij}^2$

State group[a]				N[b]	Spin states of $(CO_2)^+$					
					doublet[c]			quartet[d]		
	Atom 1	Atom 2	Atom 3		$\boldsymbol{S}_{12}^2$	$\boldsymbol{S}_{13}^2$	$\boldsymbol{S}_{23}^2$	$\boldsymbol{S}_{12}^2$	$\boldsymbol{S}_{13}^2$	$\boldsymbol{S}_{23}^2$
(a)	$O(^3P_g)$	$O(^3P_g)$	$C^+(^2P_u)$	27	(1) 0	1/2	1/2	1	1/2	1/2
					(2) 1	3/2	3/2	2	3/2	3/2
(b)	$O(^3P_g)$	$O^+(^4S_u)$	$C(^3P_g)$	9	(1) 1/2	1	1/2	1/2	0	1/2
					(2) 3/2	2	3/2	3/2	1	3/2
					(3) –	–	–	5/2	2	5/2
(c)	$O^+(^4S_u)$	$O(^3P_g)$	$C(^3P_g)$	9	(1) 1/2	1/2	1	1/2	1/2	0
					(2) 3/2	3/2	2	3/2	3/2	1
					(3) –	–	–	5/2	5/2	2

[a] The ordering of state groups and atoms is kept throughout the paper. [b] N denotes the number of space functions. [c] The total number of DIM basis functions is 90 for doublet states. [d] The total number of DIM basis functions is 108 for quartet states.

equivalent new functions, being eigenfunctions of a different diatomic-fragment spin-square operator, $\boldsymbol{S}_{13}^2$ or $\boldsymbol{S}_{23}^2$, preserving spin adaptation with respect to total spin. Table I characterizes DIM models for the total doublet and quartet states from the viewpoint of all resulting diatomic fragment spin states, which together with the spatial parts, determine completely the list of diatomic states (see Table II) playing role in the construction of the DIM polyatomic Hamiltonian matrix. One observes that despite the small atomic basis set entering the DIM model, due to relatively large multiplicities (leading to an extensive coupling scheme) and non-zero angular momentum quantum numbers of atomic states, the spatial and spin parts combine to the total of 90 doublet- and 108 quartet-adapted three-atomic VB basis functions, expressed in the short-hand form

$$\mathrm{TBF} \approx [m(1),m(2),m(3)]_{\mathrm{SG}} \times {}^{\mathrm{SG}}\sigma_j \ , \qquad (2)$$

for SG equal to (a), (b) or (c), and label j associated with spin functions.

TABLE II
Diatomic states information required as input for the DIM models of $(CO_2)^+$

Species	States	$(CO_2)^+$		Source	Representation
		doublet	quartet		
O_2	$^1\Sigma_g^+(1,2)$, $^1\Sigma_u^-$, $^1\Pi_g$, $^1\Pi_u$, $^1\Delta_g$	yes	no	ref.[20]	pointwise
	$^3\Sigma_u^+(1,2)$, $^3\Sigma_g^-$, $^3\Pi_g$, $^3\Pi_u$, $^3\Delta_u$	yes	yes	ref.[20]	pointwise
	$^5\Sigma_g^+(1,2)$, $^5\Sigma_u^-$, $^5\Pi_g$, $^5\Pi_u$, $^5\Delta_g$	no	yes	ref.[20]	pointwise
O_2^+	$^2\Sigma_g^+$, $^4\Sigma_u^+$, $^4\Pi_g$	yes	yes	AIM	pointwise
	$^2\Sigma_u^+$, $^4\Sigma_g^+$, $^2\Pi_g$, $^2\Pi_u$, $^4\Pi_u$	yes	yes	refs[21,22]	Morse curve
	$^6\Sigma_g^+$, $^6\Pi_g$, $^6\Pi_u$	no	yes	AIM	pointwise
	$^6\Sigma_u^+$	no	yes	ref.[21]	Morse curve
CO	$^3\Sigma^+(1,2)$, $^5\Sigma^+(1,2)$, $^3\Pi(1,2)$, $^5\Pi(1,2)$	yes	yes	ref.[23]	pointwise
	$^3\Sigma_u^-$, $^5\Sigma_u^-$, $^3\Delta$, $^5\Delta$	yes	yes	ref.[23]	pointwise
	$^1\Sigma^+(1,2)$, $^1\Pi(1,2)$, $^1\Sigma^-$, $^1\Delta$	no	yes	ref.[23]	pointwise
CO^+	$^2\Sigma^+(1)$, $^2\Sigma^-(1)$, $^4\Sigma^+(1)$, $^4\Sigma^-(1)$	yes	yes	refs[22,24]	Morse curve
	$^2\Pi(1)$, $^4\Pi(1)$, $^2\Delta$, $^4\Delta$	yes	yes	refs[22,25]	Morse curve
	$^2\Sigma^+(2)$, $^2\Sigma^-(2)$, $^4\Sigma^+(2)$, $^4\Sigma^-(2)$	yes	yes	AIM	pointwise
	$^2\Pi(2,3)$, $^4\Pi(2,3)$	yes	yes	AIM	pointwise
	$^6\Sigma^+$	no	yes	ref.[24]	Morse curve
	$^6\Pi$	no	yes	AIM	pointwise

With the exception of a methodological study on the stability of the DIM solution for the H + H_2 system[26], the DIM polyatomic basis sets for $(CO_2)^+$ have the largest sizes ever applied to a chemical problem. Despite this fact, caution concerning the complete adequacy of the DIM models for $(CO_2)^+$ is appropriate, because of the minimum atomic basis set condition which entails specific limitations: The models preclude the occurrence of negative charge on any of the atoms, and do not exhibit correct dissociation limits for certain excited electronic atomic states.

Table II also presents the entire numerical representation of diatomic potential energy curves (PECs) serving as input to the DIM models. We used that available PEC information which seemed to be physically as consistent as possible for the whole manifold of diatomic states created from given atomic states. For the calculation of PECs of some excited diatomic states not available in the literature, and mixing coefficients related to the fragment manifolds of the same symmetry, the symmetrically orthogonalized version[27,28] of the atoms-in-molecules (AIM) method[29] was used. The AIM atomic eigenfunctions of O and C species were represented in terms of 1s, 2s and 2p AOs, expressed by means of the 7s3p basis of Whitman and Hornback[30]. The neutral and ionic approximate atomic eigenfunctions were built up from the same AOs, the experimental energies of atomic states, providing atomic correction terms for the AIM calculations were estimated from data of ref.[31]. The AIM PECs and mixing coefficients of the CO^+ $\{^{2,4}\Sigma^+$ (2×), $^{2,4}\Sigma^-$ (2×), $^{2,4}\Pi$ (3×) $\}$, CO $\{^{1,3,5}\Sigma^+$ (2×), $^{1,3,5}\Pi$ (2×)$\}$ and O_2 $\{^1\Sigma_g^+$ (2×), $^3\Sigma_u^+$ (2×), $^5\Sigma_g^+$ (2×)$\}$ for multiple states of the same symmetry species were obtained by the VB AIM calculations performed within the corresponding symmetry-adapted restricted diatomic basis sets[32]. The spin- and space-symmetry aspects of constructing the DIM matrix, the realization of its numerical representation for given geometries, and finally the diagonalization of the resultant Hamiltonian matrix were treated by computer codes using the formalism described in ref.[33]. To obtain the diatomic interactions given pointwise as a continuous function of internuclear separation, the PECs and mixing coefficients entering the DIM model have been represented by spline fits whose knots are the internuclear separations at which diatomic calculations were performed.

RESULTS AND DISCUSSION

DIM Correlation Diagrams for Low-Lying Potential Energy Surfaces of $(CO_2)^+$

The behaviour of the $(CO_2)^+$ system at the dissociation limits to diatomic fragments is shown in Fig. 1 which also serves the purpose to show which of the significantly bound diatomic states of given fragments enter the DIM models. The zero of energy lies at –187.6663 hartree, corresponding to separated atomic species 2 O(^3P_g) and $C^+(^2P_u)$. Figure 1 also expresses the fact that the spin couplings available for fragments in the

defined DIM models preclude the participation of the CO singlet (diatomic) states in the total doublet state, and O_2 singlet (diatomic) states in the total quartet state.

The DIM correlation diagram for the doublet states connecting the reagents of $C^+(^2P_u) + O_2(^3\Sigma_g^-)$ with the products $O(^3P_g) + CO^+(^2\Sigma^+)$ *via* an insertion pathway and a collinear $(COO)^+$ abstraction pathway is shown in Fig. 2. First it is of primary interest to perform a comparison with correlation diagrams in the literature[15–17] and an evaluation in the light of available *ab initio* information on $(CO_2)^+$ PESs, which for given purpose is collected in Fig. 3. In this figure the electronic ground and excited energy levels of collinear $(OCO)^+$, including the qualitative behaviour of states (splitting and energy variation) under bending motion of the species[34], and some our own CISD results[35] (*cf.* Table III) are presented. The low-lying limits for dissociation to diatomic

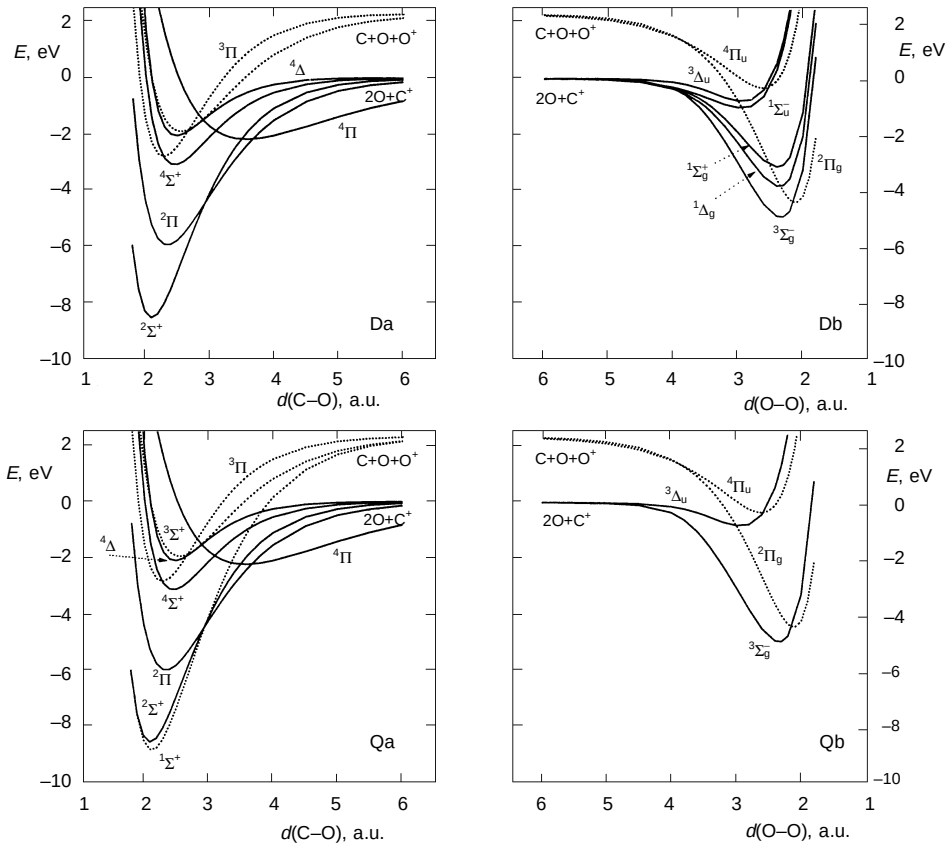

FIG. 1

Cuts through the asymptotic regions of the doublet (D) and quartet (Q) $(CO_2)^+$ DIM PESs corresponding to the strongest bound diatomic CO (CO^+) (a) and O_2 (O_2^+) (b) species

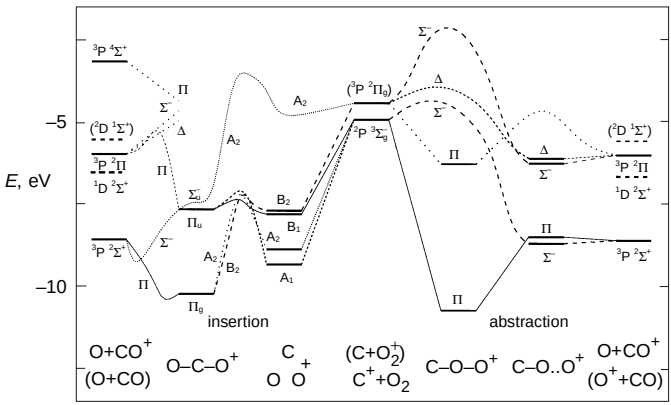

FIG. 2
DIM correlation diagram for the doublet states of $(CO_2)^+$ connecting the reagents (middle) with the products *via* insertion (left) and collinear abstraction (right) pathways

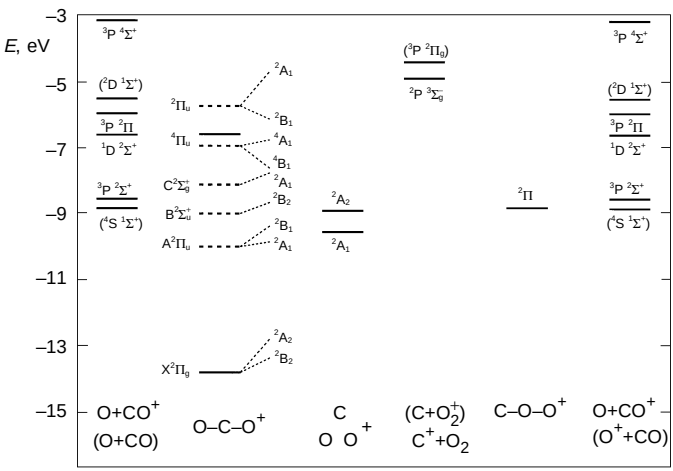

FIG. 3
External information on energy doublet levels in $(CO_2)^+$ taken from ref.[34] (dashed), and calculated[35] by using CISD (6-31G* AO basis) (solid). Dissociation limits are shifted to those corresponding to the DIM model

fragments are adapted here to input information on atomic and diatomic state information for the DIM model, enabling to set up the energy relationship between the dissociation limits and bent $(CO_2)^+$ structures.

Globally, Fig. 2 and the diagram presented by Burley and Armentrout[17] exhibit the same adiabatic linking of reagent and product states, with the exception of situations which are associated with atomic terms lying beyond the DIM minimum atomic basis set. States missing in the DIM model are shown in the region of the product states in Fig. 2 as thick dashed straight lines. The lack of a greater number of VB structures in the DIM model, especially of the $O(^1D_g) + CO^+(^2\Sigma^+)$ structure, has, of course, consequences on the behaviour of excited states which is best demonstrated in the collinear region of the insertion path: (i) The DIM $A^2\Pi_u$ state does not converge to $O(^1D_g) + CO^+(^2\Sigma^+)$, as it should, but to the $O(^3P_g) + CO^+(^2\Pi)$ asymptote, which is the genuine limit of the next higher $^2\Pi_u$ state of $(CO_2)^+$. Correspondingly, the DIM $A^2\Pi_u$ state yields the same splitting pattern as the true second $^2\Pi_u$ state, whereas the true $A^2\Pi_u$ state produces a reverse order of $^2A_1$ and $^2B_1$ levels at bending, as can be seen by comparing Figs 2 and 3. (ii) There is no appropriate asymptote for the $B^2\Sigma_u^+$ state, and no sufficient interaction with structures to raise the $^2\Sigma^-$ state emanating from the $O(^3P_g) + CO^+(^2\Sigma^+)$ asymptote, so that within the DIM model, $^2\Sigma_u^-$ becomes the electronic second excited state at collinear $(OCO)^+$ configuration.

In accordance with earlier investigations[17], the DIM model predicts that only one of three doublet surfaces connects the ground state (GS) reactants with the GS products

TABLE III
Characteristics of some local ground state minima of collinear and C_{2v} arrangements of the $(CO_2)^+$ system as obtained by the CISD *ab initio* calculations[a]

State	Configuration	Energy hartree	Interatomic separations bohr		Atomic charges a.u.		
			$d(C–O^1)$	$d(O^1–O^2)$	C	O^1	O^2
$^2\Pi$	$D_{\infty h}$, O^1 C O^2	–187.6176	2.220	4.440	0.95	0.03	0.03
$^2\Pi$	$C_{\infty v}$, C O^1 O^2	–187.4342	2.212	2.638	0.63	0.01	0.35
$^2A_2$	C_{2v}	–187.4375	2.625	2.575	0.69	0.15	0.15
$^2A_1$	C_{2v}	–187.4608	2.361	3.222	0.88	0.06	0.06
$^4\Pi$	$D_{\infty h}$	–187.3517	2.403	4.806	0.64	0.18	0.18
$^4B_2$	C_{2v}	–187.3310	2.622	2.598	0.71	0.14	0.14
CO^+ ($^2\Sigma^+$) + O		–187.4242[b]	–	–	–	–	–

[a] Ref.[35], 6-31G* AO basis, including size-consistency correction. [b] Approximate value for the dissociation limit taken as the average of doublet and quartet energy values at large separation of O from CO^+

via insertion. The point of lowest energy is reached at a symmetry broken $C_{\infty v}$ nuclear configuration, lying 0.17 eV below the $D_{\infty h}$ symmetry restricted minimum. It is noteworthy that symmetry breaking of the $^2\Pi_g$ state of $(CO_2)^+$ is well known from *ab initio* calculations[36], the barrier to the symmetric nuclear configuration taking the values 0.62 and 0.06 eV with RHF and CEPA calculations, respectively.

On the other hand, the topographical behaviour of the DIM surfaces represented by Fig. 2 is in some respects qualitatively different from that corresponding to the PESs used in previous interpretations. As C^+ approaches O_2 along the perpendicular bisector of the bond, according to ref.[17] all surfaces exhibit energy barriers in the entrance channel before smoothly dropping to the potential energy wells of the collinear stable species. The corresponding DIM surfaces, however, predict the approach to be attractive from the very beginning until reaching minima at isosceles triangle configurations, which are separated from the deep well of the collinear species by means of barriers of different height. From the view of earlier expectations[17,34], the existence of the DIM stationary points at C_{2v} configurations and the order of levels, *i.e.* finding the $^2A_1$ state to lie below the $^2A_2$ and $^2B_2$ states, are also controversial.

Without doubt, these DIM results have to be taken into consideration with great caution. Although the order of the two lowest electronic states at $D_{\infty h}$ symmetry comes out well, the binding is strongly underestimated. In fact, for regions of high symmetry there is always potential danger of failure of a DIM model, because there are basis functions (strongly limited in number) scattered to a large number of irreducible representations, thus decreasing the flexibility of the state vectors compared to regions of lower symmetry. Consequenly, the binding in C_{2v} species could be exaggerated compared to the collinear ones, possibly affecting both the relative position and the barrier height between the intermediates.

Figure 3 also testifies to the fact that information on energy data specifying the collinear $(COO)^+$ abstraction pathway is scarce. There is, however, a firm conviction[18] that a minimum at this type of conformation exists. In Fig. 2 we see that with the DIM model the minimum comes out in an exaggerated form, positioned on the $^2\Pi$ surface connecting the GS reactants and the GS products, without a barrier in the entrance channel.

The DIM correlations for the quartet states are presented in Fig. 4. The branch of the diagram connecting the GS $C^+ + O_2$ and $C + O_2^+$ reactants with GS O^+ and CO^+ product channels *via* insertion pathways shows high barriers in the entrance channel, with the exception of the $^4A_1$ state which becomes a component of the $^4\Pi_u$ state, and as a $^4\Pi$ state merges into the $O(^3P_g) + CO^+(^2\Sigma^+)$ asymptote. The DIM $^4\Pi_u$ level, however, appears to be unrealistically low, *i.e.* too close to the energy of the DIM $^2\Pi_g$ state. An appreciable difference in the behaviour of doublet and quartet states is found in the collinear $(COO)^+$ abstraction pathway: Quartet surfaces exhibit no binding with respect

to GS products, and all quartet surfaces correlating with the products display substantial barriers either in the entrance or exit channels.

Correlation of Topographical Features and DIM Wave Function Composition

It is difficult to rationalize the topographical behaviour of the DIM PES in terms of particular diatomic interactions, because the spin-coupling and the rotational properties of the atomic functions in the direct-product basis set intricately hide the desired information in the wave function. It appears, however, useful to characterize the DIM wave function at a given geometrical arrangement in terms of contributions from VB structures associated with individual SGs and spin-coupling structures, since the composition of such contributions in the wave function is invariant with respect to the choice of the coordinate system.

In Table IV the VB-structure character of doublet and quartet ground state wave functions at important nuclear configurations of the $(CO_2)^+$ system is presented. This table reveals that VB structures pertinent to SG (a), *i.e*. with the positive charge residing on the carbon atom, are primarily responsible for the bonding properties of both the ground doublet and quartet states. Notice now from Table I that the spin-coupling schemes (1) and (2) of SG (a) differ for both multiplicities in the behaviour only with respect to $\boldsymbol{S}_{12}^2$, *i.e*. that spin-square operator associated with the OO fragment, corresponding to the remotest atoms in the collinear $(OCO)^+$ configurations. Thus, the similar behaviour of the total doublet and quartet surfaces at collinear $(OCO)^+$ configurations can be explained on grounds of equal CO^+ diatomic interactions, primar-

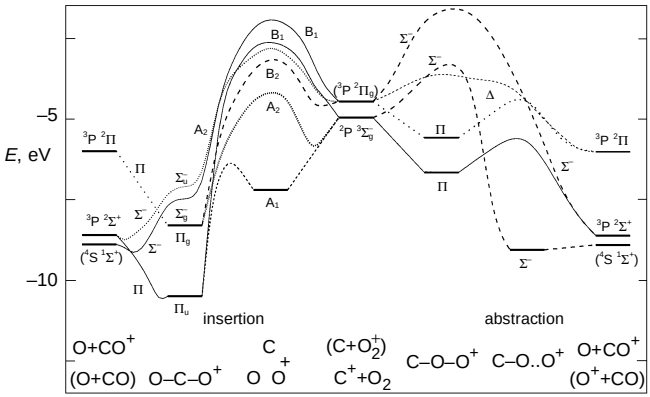

FIG. 4
DIM correlation diagram for the quartet states of $(CO_2)^+$ connecting the reagents (middle) with the products *via* insertion (left) and collinear abstraction (right) pathways

ily responsible for binding in this configuration (see Fig. 1). The likeness of both types of PESs is also manifested in Table IV by the fact that the partitioning of the weight of SG (a) into spin-coupling schemes (1) and (2) is much the same for the doublet and quartet states of $(CO_2)^+$ at the minimum which is restrained to $D_{\infty h}$ symmetry. Notice further that at this centrosymmetric configuration the dominant structures stem from spin-coupling type (2) of SG (a) which enforces quartet CO^+ interactions. Departure from symmetric to unsymmetric collinear configurations loosens symmetry restrictions for participation of TBFs in the wave function expansion, particularly favouring additional TBFs of spin-coupling type (1). This distortion allows the strongest bound $^2\Sigma^+$ diatomic interaction (*cf.* Fig. 1) to come into more pronounced effect and influence the bonding in the whole system. Indeed, at unsymmetric $(O\text{--}C\text{-}O)^+$ configurations the role of the spin-coupling scheme (1) increases in the total wave functions of both multiplicities with respect to the symmetric configurations, the effect being greater with the doublet state, as it corresponds to the more pronounced symmetry-breaking effect (see Table IV). The influence of the Σ^+ (CO^+) potentials on the features of the $(CO_2)^+$ PESs can be used as the remedy for the symmetry-breaking phenomenon in the DIM solution: Optimization of mixing[12,14] between diatomic structures $O(^3P_g).C^+(^2P_u)$ and $O^+(^4S_u).C(^3P_g)$ with respect to the minimization of the symmetry-breaking effect

TABLE IV
DIM wave function analysis in terms of VB structures in doublet and quartet states of $(CO_2)^+$ at important stationary points (*cf.* text)

		Doublet			Quartet	
Energy, eV		–10.23	–10.39	–10.73	–10.50	–10.55
Configuration[a]		O.C.O	$O^2.C..O^1$	$C.O^2.O^1$	O.C.O	$O^2.C..O^1$
State group	Spin function	Weight of VB structures, %				
(a)	(1)	7	16	34	12	13
	(2)	61	55	39	59	58
(b)	(1)	0	5	16	0	0
	(2)	15	16	8	5	5
	(3)	–	–	–	10	18
(c)	(1)	0	0	1	0	0
	(2)	15	8	2	5	4
	(3)	–	–	–	10	3

[a] Ordering of oxygen atoms is relevant to the classification in terms of state groups, *e.g.* O^2 is an O^+ species in SG (b) as defined in Table I.

(where, *e.g.*, $O(^3P_g)$ denotes the approximate oxygen-atom eigenfunction with appropriate quantum numbers M_L and M_S) enables an almost complete removal of the molecular symmetry breaking. This procedure is accompanied by a positive charge enhancement on the C atom at the expense of charges on atoms O, without a meaningful alteration in the topographical behaviour of the doublet and quartet ground state PESs.

Compared to the $(OCO)^+$ configurations, the role of OO interactions increases in collinear $(COO)^+$ configurations. It is seen from Table I that the total doublet state permits for the SG (a) singlet and triplet coupling in the OO fragment. The existence of well bound O_2 PECs of these both spin species (Fig. 1) offers a good chance for bonding at $(COO)^+$ configurations. For the total quartet state, however, the bonding conditions are by far less favourable, since $^3\Sigma_g^-$ (O_2) is the only well-bound diatomic state (Fig. 1) among the O_2 triplet and quintet states required in the coupling scheme (Table I). This again yields an explanation for the difference in bonding between doublet and quartet states at $(COO)^+$ configurations.

Support of the DIM Models by Simple ab initio Calculations

It is gratifying that the typical features of the DIM doublet and quartet surfaces of $(CO_2)^+$, including qualitative argumentation based on VB concepts of bonding, could be corroborated by our preliminary *ab initio* calculations. As it is seen in Table III, the *ab initio* calculations find minima at C_{2v} geometries in that order as predicted by the DIM model. In fact, within an analysis of minimum energy paths for isosceles triangle configurations, it was found that each of the three electronic states, $^2B_2$, $^2A_1$ and $^2A_2$, is becoming the ground state in certain portions of the configuration space. While the $^2B_2$ state is steadily decreasing with diminishing separation of C from the center of mass of O_2 until reaching the absolute minimum as a component of the $^2\Pi_g$ state, the $^2A_1$, and $^2A_2$ states show distinct wells at non-linear configurations. Further, the CISD calculations confirm the existence of minima on the GS doublet surface for collinear $(OCO)^+$ and $(COO)^+$ configurations, and on the GS quartet surface at centrosymmetric collinear geometry. Also pleasing is that population analysis using the CI density yields positive charges positioned on all constituent atoms for important $(CO_2)^+$ geometries given in Table III. This fact physically justifies to a certain extent the choice of our DIM-model structure taking into account only neutral and positively charged atomic species.

CONCLUSIONS

DIM model calculations focus attention to new topological features of PESs referring to reactions of the ground-state atomic carbon cation with molecular oxygen, which are in some cases contrary to PES characteristics presented in previous correlation diagrams[15–18] used to the interpretation of collision experiments so far. The basic DIM results for the ground and low-lying excited electronic states can be collected in the

following way: (i) Low-lying doublet states of $(CO_2)^+$ exhibit minima not only at the centrosymmetric collinear geometry, but also at the collinear $(OOC)^+$ and bent (C_{2v}) structures; (ii) As C^+ approaches O_2 along the perpendicular bisector of the bond, DIM predicts the PESs to be attractive from the very beginning until reaching minima at isosceles triangle configurations, separated from the deep well of the centrosymmetric species by potential energy barriers, while according to ref.[17] all PESs exhibit energy barriers in the entrance channel before smoothly dropping to wells at centrosymmetric equilibrium geometries; (iii) All quartet states connecting the ground state reagents $C^+ + O_2$ and $C + O_2^+$ with products *via* an insertion pathway show significant barriers in the entrance channel, with the exception of the $^4A_1$ state, correlating with the $^4\Pi_u$ ground state structure and merging into the $O + CO^+$ asymptote at dissociation; (iv) Numerous avoided and real intersections of doublet states (*cf.* the insertion pathway) and doublet–quartet crossings indicate the importance of non-adiabatic and spin–orbit interaction effects in this reaction, respectively. Despite the fact that the DIM model for $(CO_2)^+$ could yield only qualitative information on the course of the reaction pathways, it was found very useful in giving suggestions for application[37] of complete active space self-consistent and internally contracted multireference configuration interaction approaches, serving to elucidate the complex electronic structure and vibronic coupling in $(CO_2)^+$.

The work was supported by the Grant Agency of the Czech Republic (grant No. 203/96/0947) and by the European Network "Structure and Reactivity of Molecular Ions". The author is indebted to Prof Dr G. Chambaud and Prof. Dr P. Rosmus (Groupe de Chimie Théorique, Université de Marne la Vallee, France) for helpful discussions at all stages of the work.

REFERENCES

1. Ellison F. O.: *J. Am. Chem. Soc*. **1963**, *85*, 3540.
2. Tully J. C. in: *Modern Theoretical Chemistry. Semiempirical Methods of Electronic Structure Calculation* (G. A. Segal, Ed.), Vol. 7A, Chap. 6. Plenum, New York 1977.
3. Kuntz P. J. in: *Atom–Molecule Collision Theory. A Guide for the Experimentalist* (R. B. Bernstein, Ed.), Chap. 3. Plenum, New York 1979.
4. Kuntz P. J.: *Chem. Phys. Lett*. **1972**, *16*, 581.
5. London F.: *Z. Elektrochem*. **1929**, *35*, 552.
6. Eyring H., Polanyi M.: *Z. Phys. Chem., B* **1931**, *12*, 279.
7. Sato S.: *J. Chem. Phys*. **1955**, *23*, 592.
8. Eaker C. W., Parr C. A.: *J. Chem. Phys.* **1976**, *64*, 1322.
9. Schneider F., Zulicke L., Polak R., Vojtik J.: *Chem. Phys.* **1983**, *76*, 259.
10. Kuntz P. J., Polak R.: *Chem. Phys*. **1985**, *99*, 405.
11. Polak R., Paidarova I., Kuntz P. J.: *J. Chem. Phys*. **1987**, *87*, 2863.
12. Polak R.: *J. Mol. Struct., THEOCHEM* **1991**, *227*, 219.
13. Kendrick B., Pack R. T.: *J. Chem. Phys*. **1995**, *102*, 1194.
14. Polak R., Paidarova I., Kuntz P. J.: *Int. J. Quantum Chem*. **1997**, *62*, 659.

15. Sonnenfroh D. M., Farrar J. M.: *Chem. Phys. Lett.* **1986**, *125*, 123.
16. Rincon M., Pearson J., Bowers M. T.: *Int. J. Mass Spectrom. Ion Process.* **1987**, *80*, 133.
17. Burley J. D., Armentrout P. B.: *Int. J. Mass Spectrom. Ion Process.* **1988**, *84*, 157.
18. Wittemann A.: *Ph.D. Thesis*. Albert-Ludwigs-Universitat Freiburg, Breisgau 1994.
19. Polak R., Paidarova I., Kuntz P. J.: *J. Chem. Phys.* **1985**, *82*, 2352.
20. Saxon R. P., Liu B.: *J. Chem. Phys.* **1977**, *67*, 5432.
21. Beebe N. H. F., Thulstrup E. W., Andersen A.: *J. Chem. Phys.* **1976**, *64*, 2080.
22. Huber K., Herzberg G.: *Molecular Spectra and Molecular Structure*, Vol. 4. Van Nostrand Reinhold, New York 1979.
23. O'Neil S. V., Schaefer III H. F.: *J. Chem. Phys.* **1970**, *53*, 3994.
24. Honjou N., Sasaki F.: *Mol. Phys.* **1979**, *37*, 1593.
25. Lavendy H., Robbe J. M., Flament J. P.: *Chem. Phys. Lett.* **1993**, *205*, 456.
26. Roach A. C., Kuntz P. J.: *J. Chem. Phys.* **1986**, *84*, 822.
27. Polak R.: *Chem. Phys.* **1981**, *60*, 287.
28. Polak R., Vojtik J., Paidarova I., Schneider F.: *Chem. Phys.* **1981**, *55*, 183.
29. Moffitt W.: *Proc. R. Soc. London, Ser. A* **1951**, *210*, 245.
30. Whitman D. R., Hornback C. J.: *J. Chem. Phys.* **1969**, *51*, 398.
31. Moore C. E.: *Atomic Energy Levels*, NSRDS–NBS Circular No. 467. US GPO, Washington D.C. 1949.
32. Polak R., Vojtik J.: *Chem. Phys.* **1984**, *87*, 273.
33. a) Vojtik J.: *Int. J. Quantum Chem.* **1985**, *28*, 593; b) Vojtik J.: *Int. J. Quantum Chem.* **1985**, *28*, 943.
34. Praet M. T., Lorquet J. C., Raseev G.: *J. Chem. Phys.* **1982**, *77*, 4611.
35. Frisch M. J., Trucks G. W., Schlegel H. B., Gill P. M. W., Johnson B. G., Robb M. A., Cheeseman J. R., Keith T. A., Petersson G. A., Montgomery J. A., Raghavachari K., Al-Laham M. A., Zakrzewski V. G., Ortiz J. V., Foresman J. B., Peng C. Y., Ayala P. Y., Chen W., Wong M. W., Andres J. L., Replogle E. S., Gomperts R., Martin R. L., Fox D. J., Binkley J. S., Defrees D. J., Baker J., Stewart J. P., Head-Gordon M., Gonzales C., Pople J. A.: *GAUSSIAN 94, Revision B.3*. Gaussian Inc., Pittsburgh, PA 1995.
36. Brommer M., Chambaud G., Reinsch E.-A., Rosmus P., Spielfiedel A., Feautrier N., Werner H.-J.: *J. Chem. Phys.* **1991**, *94*, 8070; and references therein.
37. Polak R., Hochlaf M., Levinas M., Chambaud G., Rosmus P.: Unpublished results.